Electronic Supplementary Information

Dynamic surface reconstruction governs hydrogen evolution activity of Mo_2C electrocatalysts in alkaline media

Palash Jyoti Gogoi[a,b],† Chandraraj Alex[a,c], † Swetarekha Ram[d], Nikhil N. Rao[a], Muhammed Safeer Naduvil Kovilakath[a], Seung-Cheol Lee[d,e], Satadeep Bhattacharjee[d]*, Neena S. John[a,b]*

[a]*Centre for Nano and Soft Matter Sciences (CeNS), Shivanapura, Bengaluru 562162, India*

[b]*Academy of Scientific and Innovative Research (AcSIR), Ghaziabad 201002, India*

[c]*Institute of Experimental and Applied Physics, Kiel University, Germany*

[d]*Indo-Korea Science and Technology Center (IKST), Bangalore 560064, India*

[e] *Electronic Materials Research Center, Korea Institute of Science and Technology, Korea*

† Equal Contribution

1 Experimental section

1.1 Chemicals and reagents

All chemicals are reagent grade and used without further purification. Ammonium heptamolybdate tetrahydrate $(NH_4)_6\ Mo_7O_{24}.4H_2O$, 99% purity) from Merck, 65% nitric acid from Merck were used for synthesis of *h*-MoO_3. KOH (Sigma-Aldrich, ≥ 85%) was used for electrolyte preparation. $Na_2MoO_4.2H_2O$ is purchased from Sigma-Aldrich. Commercially purchased Mo_2C (std. Mo_2C) from Nanoshel (99.5% purity) is used as reference standard. 20 wt% Pt/C purchased from sigma-aldrich is used as standard HER catalyst. The precursor solutions and electrolytes were prepared using ultrapure water. Commercially available carbon black (Super P) was used as the carbon source.

1.2 Preparation of Mo_2C nanostructures

The *h*-MoO_3 was first prepared employing a modified microwave synthesis route[1] and further used as the molybdenum source for the synthesis of Mo_2C. For *h*-MoO_3 synthesis, 2.47 g of ammonium heptamolybdate tetrahydrate (AHM) was dissolved in 20 mL water and subsequently acidified with 1 mL (0.5 M) of HNO_3. Then, the mixture was transferred to a 35 mL pyrex vessel, sealed and subjected to microwave heating with continuous stirring at 180 ℃ under 200 psi pressure for 30 min (Microwave synthesizer CEM Discover 2.0). The white solid formed was collected, washed and dried and further used for carbothermal reduction. The as prepared *h*-MoO_3 (200 mg) (Fig. S1a) was ground with 100 mg of carbon black (Super P) in an agate mortar for uniform mixing. Thereafter, the mixture was loaded in a fused quartz tube heated to 730 ℃ at a ramp rate of 5 ℃/min, and held for 2 h under a continuous flow of N_2 gas in a tube furnace. The tube was allowed to cool naturally to room temperature, yielding a black product denoted as Mo_2C 730. The synthesis was also performed at three different temperatures, 460 ℃, 650 ℃, and 930 ℃ for 2 h and 930 ℃ for 4 h and the corresponding samples were denoted as MoO_2/Mo_4O_{11} 460, MoO_2 650, Mo/Mo_2C 930 2h, Mo/Mo_2C 930 4h.

2 Characterization techniques

2.1 Physical characterization

The powder X-ray diffraction (XRD) pattern was acquired employing Rigaku Smart Lab X-ray diffractometer equipped with Cu Kα (40 kV and 30 mA) incident radiation (λ=1.5406Å) in Bragg-Brentano focusing mode. Surface morphology of the catalysts was obtained using TESCAN MIRA3 LMU field emission scanning electron microscope (FESEM) equipped with the EDS detector, Bruker

Nano Flash 630 at 20 kV. Transmission electron microscopy (TEM) images and selected-area electron diffraction (SAED) patterns were captured using a Thermo Scientific Talos F200S G2 TEM instrument operated at 200 kV. X-ray photoelectron spectroscopy (XPS) measurements were performed using a Thermo Fisher K-Alpha surface analysis spectrometer equipped with an Al Kα micro-focused monochromatic X-ray source, a hemispherical analyser featuring a 128-channel detector, and a dual-beam charge neutralization mechanism. The percentage of Mo metals in the electrolyte and catalysts was analysed using inductively coupled plasma-optical emission spectroscopy (ICP-OES) (iCAP 6300 Duo, Thermo Fisher).

2.2 *In situ* Raman spectroscopy

In situ Raman spectroscopy was performed using Horiba Jobin Yvon XploRA PLUS V1.2 MULTILINE equipped with a CCD 1024 × 256 chip detector. The spectra were acquired employing a 532 nm (25 mW) laser source with power adjusted to 12.5 mW. The sample surface is focused using a long working distance 50x objective lens, 1200 lines mm^{-1} grating for an acquisition time of 30 s and accumulation of 2. LabSpec6 spectral software was used for Raman spectra acquisition and analysis. Prior to *in situ* experiments, the Raman spectrometer was calibrated with respect to a silicon reference at 520.5 ± 0.2 cm^{-1}. A custom designed electrochemical cell with catalyst coated carbon paper as the working electrode, graphite rod as the counter electrode and Hg/HgO as the reference in a three-electrode configuration was employed and the cell was connected to a potentiostat (CHI 760 E) to apply potential (Fig. S12a). The catalyst ink was drop-cast on to the carbon paper (1×1 cm^2, mass loading of 0.4 mg cm^{-2}). Raman signals were collected at open circuit potential (OCP) in 1 M KOH followed by applied HER potential of −0.25 V vs RHE at different time intervals.

2.3 X-ray absorption spectroscopy analysis

X-ray absorption spectroscopy (XAS) measurements were carried out at Deutsches Elektronen-Synchrotron (DESY), Petra III P64 beamline at Hamburg, Germany. X-ray absorption near edge structure (XANES) and extended X-ray absorption fine structure (EXAFS) of Mo K-edge in the fluorescence mode were acquired employing a Si(111) double crystal monochromator and passivated implanted planar diode (PIPS) detector. *In situ* XAS experiments were performed using an acrylate-made, customized spectro-electrochemical cell in a three-electrode configuration as shown in (Fig. S11a). The cell consists of a Kapton window that is transparent to X-rays, with the catalyst-coated carbon fibre paper (working electrode) positioned close to the window to minimize the volume of the electrolyte between the Kapton window and the catalyst surface. The Hg/HgO and graphite are used as reference and counter electrodes. *In situ* XAS data was collected while performing current vs time *(i-t)* at the HER potential. *Ex situ* XAS spectra of the catalysts before and after the stability tests were acquired from pellets of the samples in *h*-BN matrix and the right mass of the catalysts was calculated from the xafsmass software. The processing of the XANES data background correction, alignment and normalization were performed using ATHENA software. Artemis software is used to analyse extended X-ray absorption fine structure (EXAFS) data.

2.4 Electrochemical measurements

The catalyst (2 mg) under investigation was dispersed in a mixture of 200 μL of DMF and 50 μL of 2 wt% Nafion ink by sonication for half an hour to make homogeneous catalytic ink. Five μL of catalytic ink was coated onto a glassy carbon electrode (GCE). For commercial Mo_2C catalyst 15 μL (1 mg/mL) of super P (conductive carbon) was added to catalyst ink. The carbon paper electrodes were prepared by coating 71 μL of the same ink. The catalysts loading on GCE is ~40 μg and on carbon paper is 0.57 mg cm^{-2}. The calculation details of mass loading of the catalysts are provided below. The actual amount of Mo loading on carbon paper for all the three catalysts are calculated from ICP-OES measurements. All electrochemical measurements were performed using a CHI 760E electrochemical workstation

fitted with a three-electrode system wherein the modified GCE or carbon paper served as the working electrode, graphite rod as the counter electrode and Hg/HgO (1 M NaOH) as the reference electrode. The HER performance was recorded by linear sweep voltammetry (LSV) at a scan rate of 5 mVs^{-1} in 1 M KOH using a modified GCE. The *i-t* (chronoamperometry) plots were monitored using catalyst coated on carbon paper (1 cm^2 catalyst coated area). Electrochemical impedance data was acquired in the frequency range from 10^{-1} to 10^4 Hz, applying a sinusoidal AC wave of ± 5 mV in 1 M KOH.

Mass loading calculation in Glassy carbon electrode (GCE) and carbon paper

Volume of Catalyst ink = 250 µL

Amount of catalyst in the prepared ink = 2 mg

Drop-casted amount on GCE (0.07 cm^2) = 5 µL

Mass loading on GCE = $\frac{2\ mg\ \times 5\ \mu L}{250\ \mu L} \approx 40$ µg

Drop-casted amount on Carbon paper (1 × 1 cm^2) = 71 µL

Mass loading on Carbon paper = $\frac{2\ mg\ \times 71\ \mu L}{250\ \mu L}$ = 0.57 mg cm^{-2}

Mo loading on carbon paper from ICP-OES

Mo_2C 730 = 374 µg

Mo/Mo_2C 930 2h = 434 µg

Mo/Mo_2C 930 4h = 536 µg

Supporting Data

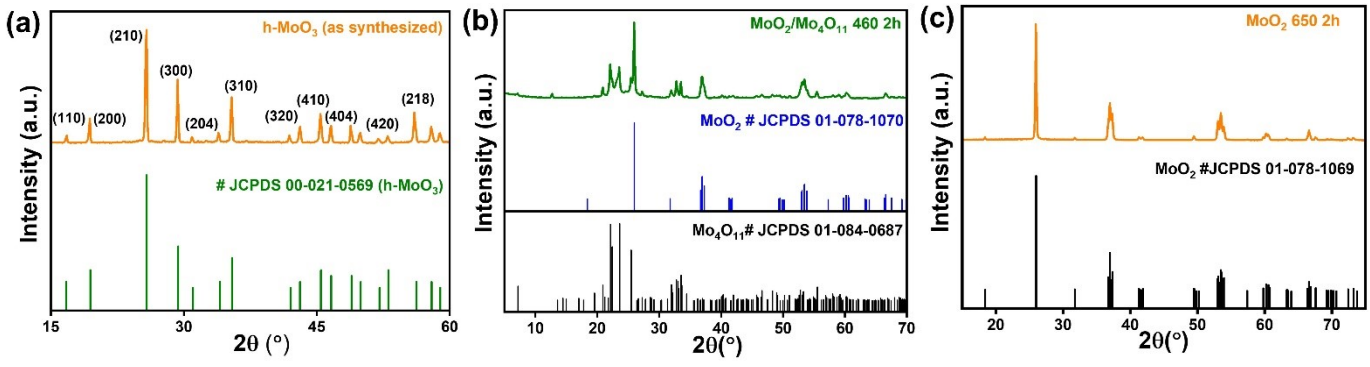

1. XRD data of *h*-MoO_3 and material synthesized at 460 °C and 650 °C

Figure S1. *(a) XRD patterns of h-MoO_3 prepared by microwave route. XRD pattern of materials formed during carbothermal reduction at (b) 460 °C and (c) 650 °C.*

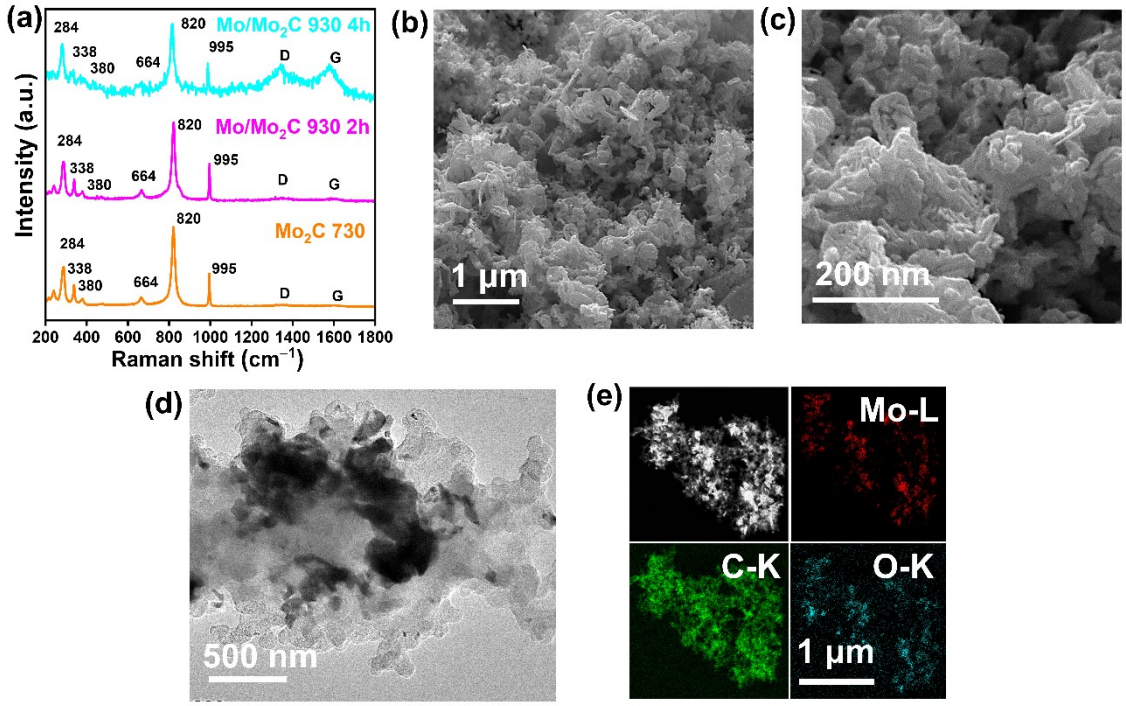

2. FESEM and TEM image of Mo_2C 730

Figure S2. *(a) Raman spectra of Mo_2C 730, Mo/Mo_2C 930 2h, Mo/Mo_2C 930 4h, (b) & (c) FESEM micrographs and (d) TEM image of Mo_2C 730 (e) HADDF image and TEM-EDS elemental mapping of Mo2C 730 (Mo-L, red; C-K, green; O-K, cyan).*

3. FESEM images of Mo/Mo_2C 930 2h and Mo/Mo_2C 930 4h

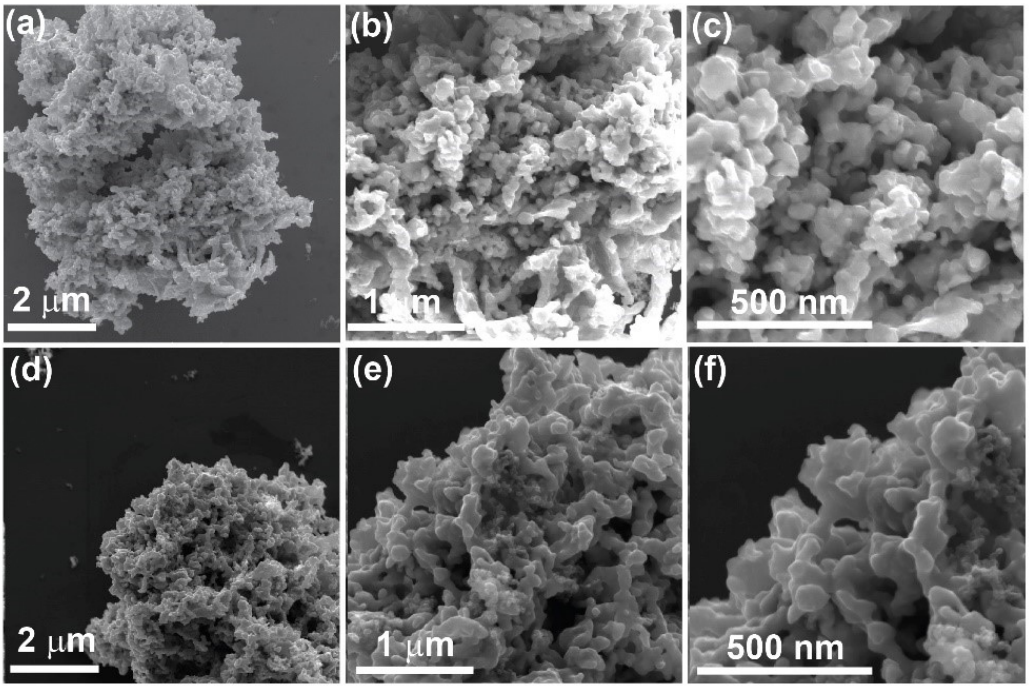

Figure S3. *FESEM micrographs (a-c) Mo/Mo_2C 930 2h (d-f) Mo/Mo_2C 930 4h.*

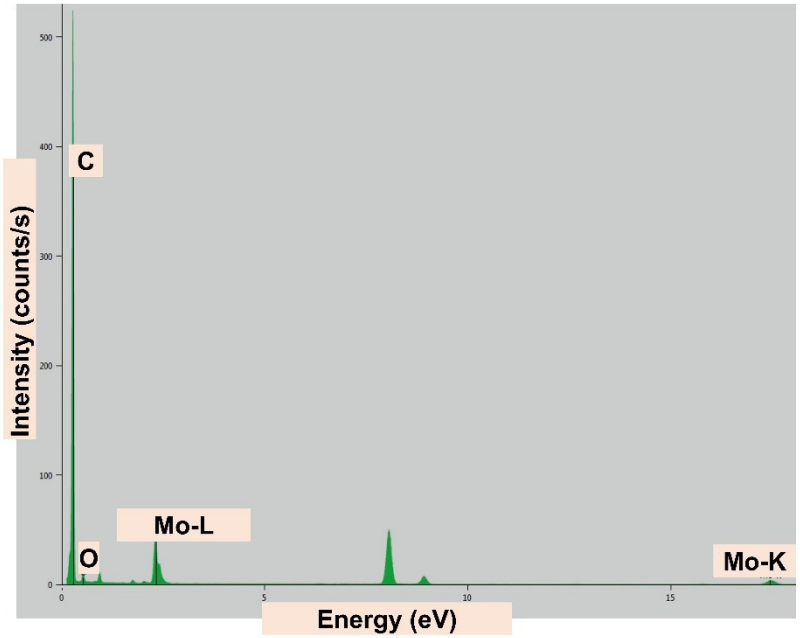

4. TEM-EDS elemental distribution

Figure S4. *TEM-EDS analysis of Mo_2C 730 showing the atomic percentage of the constituent elements Mo, C, O.*

Table S1. *Elemental composition of Mo_2C 730 from TEM-EDS*

Atomic percentage of each element of Mo_2C 730		
Mo	**C**	**O**
7.35%	91.9%	1.36%

5. Mo K-edge XANES of Mo_2C catalysts

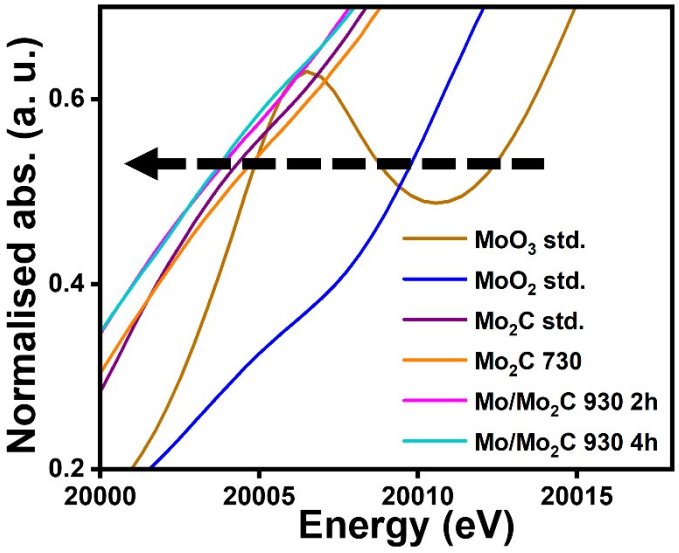

Figure S5. *Expanded view of Mo K-edge XANES of Mo_2C 730, Mo/Mo_2C 930 2h, Mo/Mo_2C 930 4h with standards.*

6. Linear combination XANES fitting

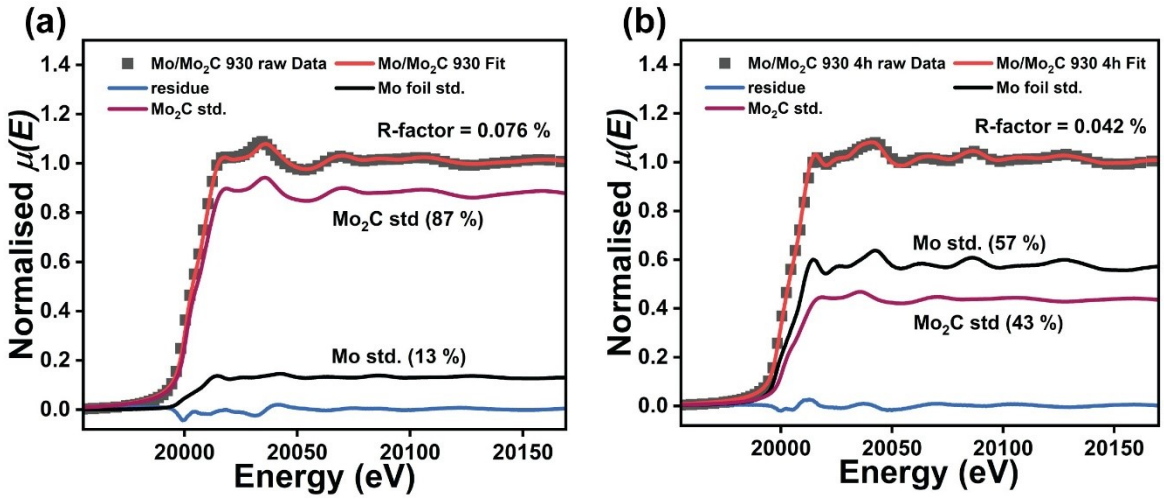

Figure S6. *Linear combination fitting of (a) Mo/Mo_2C 930 2h, (b) Mo/Mo_2C 930 4h XANES data.*

7. X-ray photoelectron spectroscopy

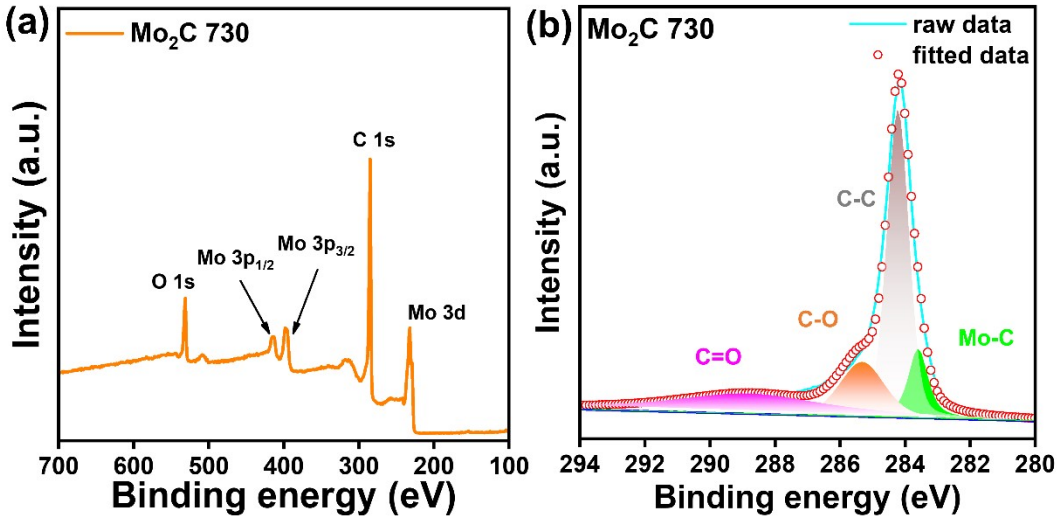

Figure S7. *(a) XPS survey spectra (b) C1s spectra of Mo_2C 730*

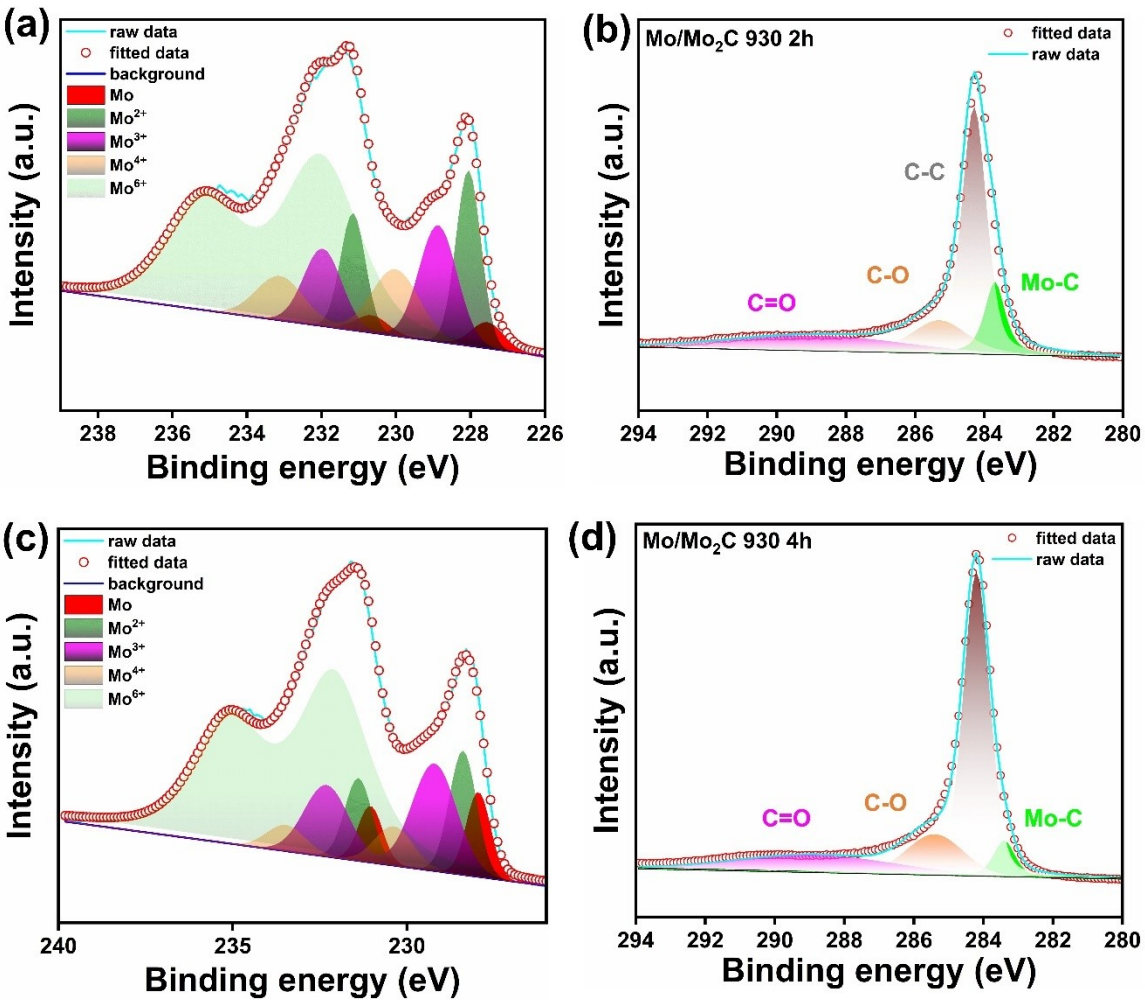

Figure S8. *XPS spectra (a) Mo 3d and (b) C1 s of Mo/Mo_2C 930 2h (c) Mo 3d and (d) C 1s of Mo/Mo_2C 930 4h.*

Table S2. *Surface elemental composition of Mo species and their relative percentages for Mo_2C 730, Mo/Mo_2C 930 2h, Mo/Mo_2C 930 4h*

Samples	Species	B.E (eV) Mo $3d_{5/2}$	B.E (eV) Mo $3d_{3/2}$	Content of Mo species (%)
Mo_2C 730	Mo^{2+}	228.26	231.31	23.56
	Mo^{3+}	229.04	232.04	20.28
	Mo^{4+}	229.74	232.74	22.70
	Mo^{6+}	232.05	235.05	33.49
Mo/Mo_2C 930 2h	Mo^{0}	227.55	230.65	15.37
	Mo^{2+}	228.06	231.16	19.03
	Mo^{3+}	228.88	231.98	19.07

	Mo^{4+}	230.05	233.15	17.78
	Mo^{6+}	232.05	235.15	28.73
Mo/Mo_2C 930 4h	Mo^0	227.95	231.05	16.92
	Mo^{2+}	228.39	231.39	18.21
	Mo^{3+}	229.22	232.52	19.52
	Mo^{4+}	230.38	233.48	16.44
	Mo^{6+}	232.1	235.1	28.90

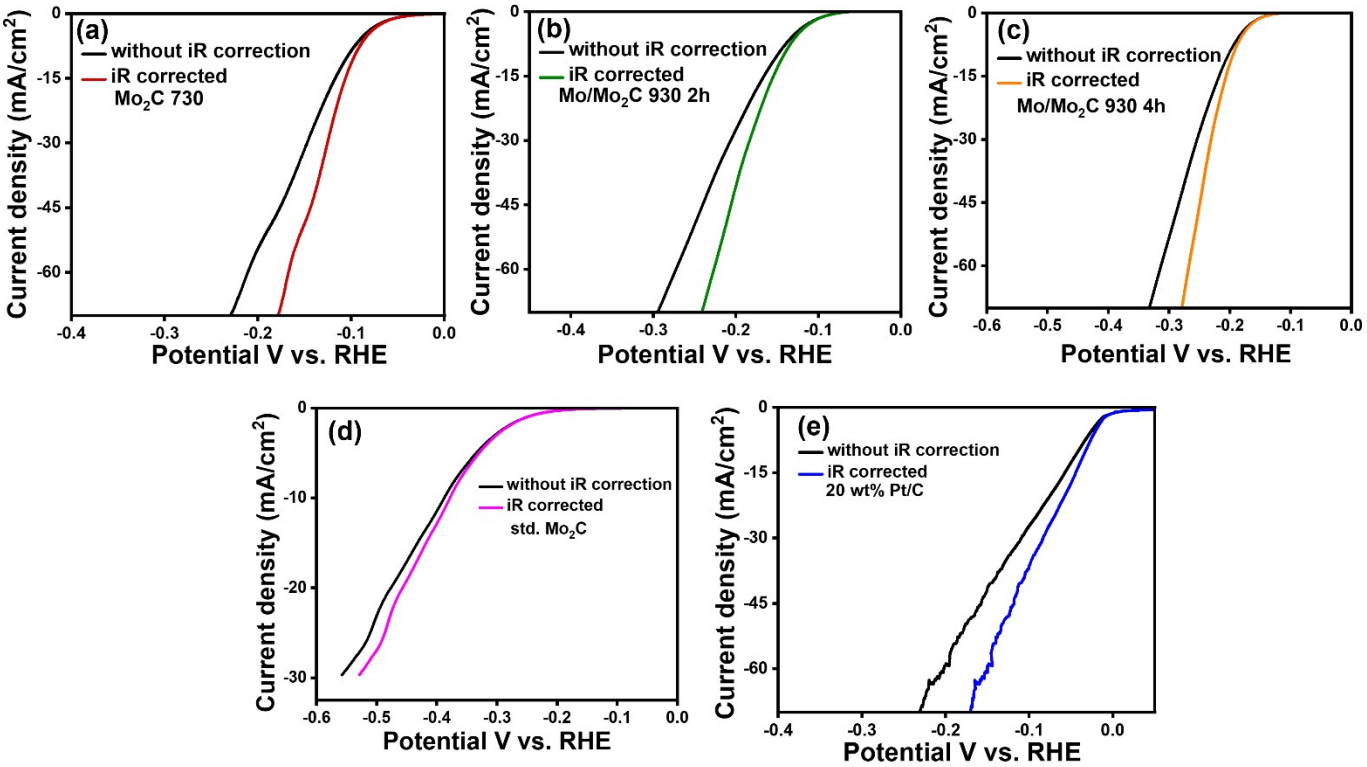

8. iR corrected and uncorrected LSVs

Figure S9. *iR corrected and uncorrected LSV of (a) Mo_2C 730 (b) Mo/Mo_2C 930 2h (c) Mo/Mo_2C 930 4h (d) std. Mo_2C (e) 20 wt% Pt/C.*

9. Chronoamperometry (i-t) for 20 h

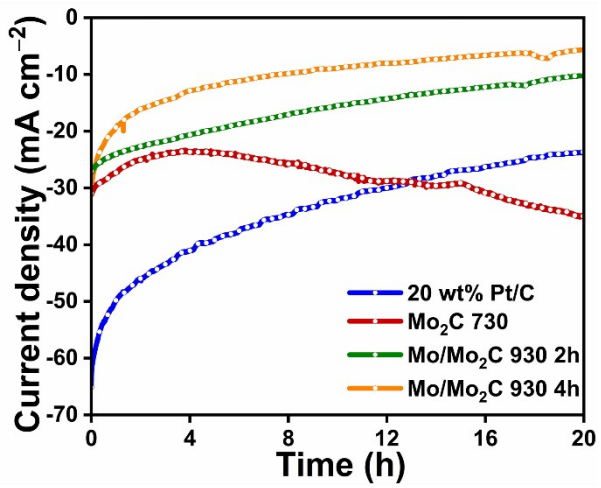

Figure S10. *Chronoamperometry plots of Mo_2C 730, Mo/Mo_2C 930 2h, Mo/Mo_2C 930 4h and 20 wt% Pt/C.*

10. Impedance fitting details at −0.25 V vs. RHE

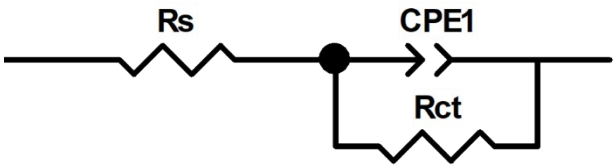

Figure S11. *Equivalent circuit for impedance data of Mo_2C 730, Mo/Mo_2C 930 2h and Mo/Mo_2C 930 4h.*

Table S3. *Fitted data from impedance spectroscopy analysis*

Catalysts	R_s (Ω)	R_{ct} (Ω)	CPE 1-T (F)	CPE 1-P (F) (10^{-3})	χ^2 (10^{-2})
Mo_2C 730	17.33	29.59	2.7525 × 10^{-4}	0.80	0.6977
Mo/Mo_2C 930 2h	17.58	45.37	1.1667 × 10^{-4}	0.67	1.52
Mo/Mo_2C 930 4h	17.71	108.9	3.3742 ×	0.80	0.6643

			10^{-4}		
Comm. Mo_2C	16.49	270.26	2.7831×10^{-5}	0.74	0.06649

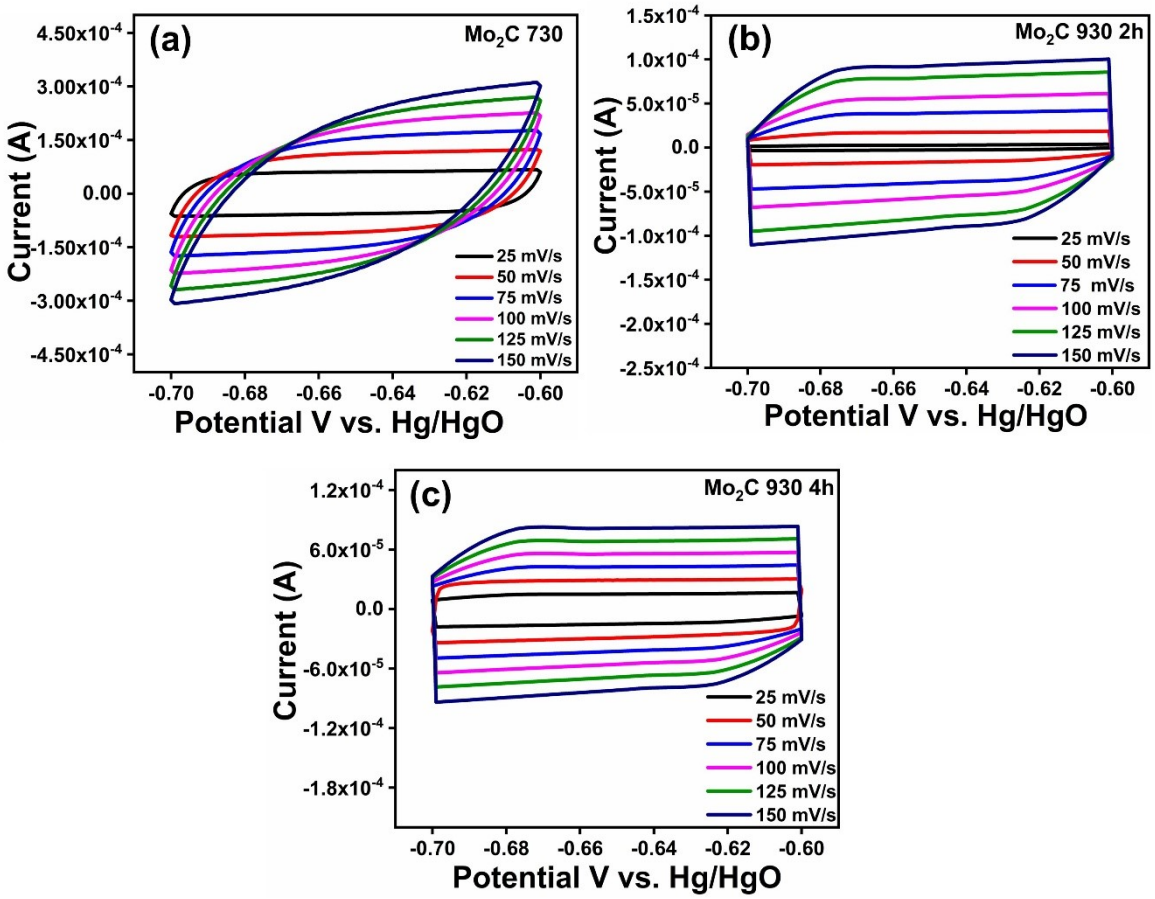

11. ECSA calculation

Figure S12. *Cyclic voltammograms of (a) Mo_2C 730 (b) Mo/Mo_2C 930 2h (c) Mo/Mo_2C 930 4h in non-faradic region (−0.6 V to −0.7 V vs. Hg/HgO).*

To measure electrochemically active surface area, CV curves are recorded in a potential range between −0.6 V to −0.7 V vs. Hg/HgO (in the double layer region where no faradaic process is observed) at a different scan rate (Figure S11θ (a), (b), (c)) and capacitive current ($\Delta j = (j_{anodic} - j_{cathodic})/2$) at an applied potential of −0.65 V (vs. Hg/HgO) is used to estimate the double layer capacitance (C_{dl}).

ECSA can be estimated by dividing the C_{dl} by standard specific capacitance (C^*). The specific capacitance of standard Mo_2C material is chosen as 40 μFcm^{-2}. [2]

$$A_{ECSA} = \frac{C_{dl}}{C^*}$$

So, ECSA values for Mo_2C 730, Mo/Mo_2C 930 2h and Mo/Mo_2C 930 4h are 31.75 cm^2, 18.2 cm^2, 13.1 cm^2.

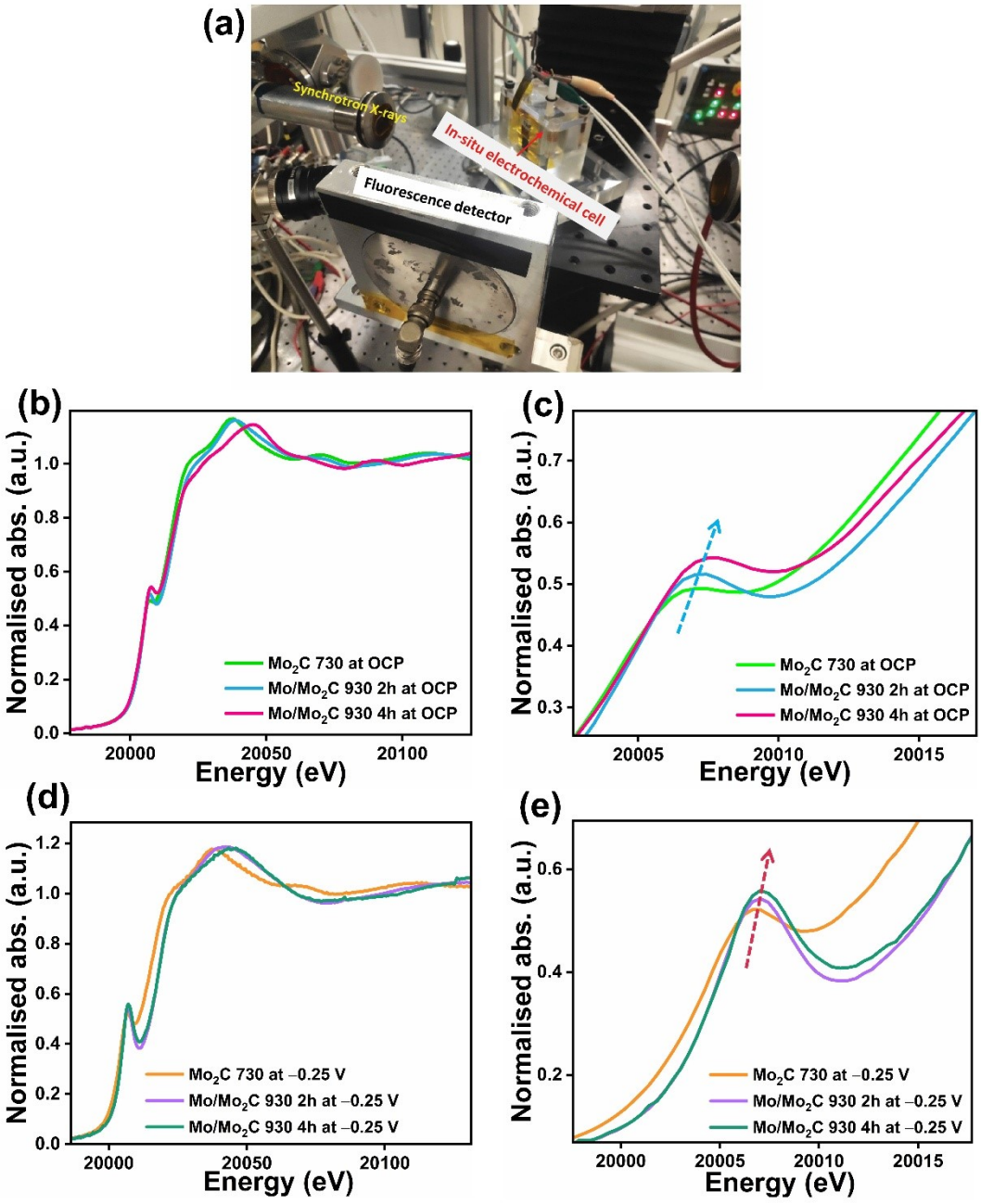

12. Mo K-edge XANES at OCP and at HER potential from *in situ* XAS data

Figure S13. *Photographs of in situ XAS set-up at Petra III, DESY (a), Mo K-edge XANES of Mo_2C 730, Mo/Mo_2C 930 2h and Mo/Mo_2C 930 4h catalysts (b) at OCP and (c) Magnified view of (b), (d)at HER potential, −0.25 V and (e) magnified view of (d) (arrows represent increment of pre-edge) in 1 M KOH.*

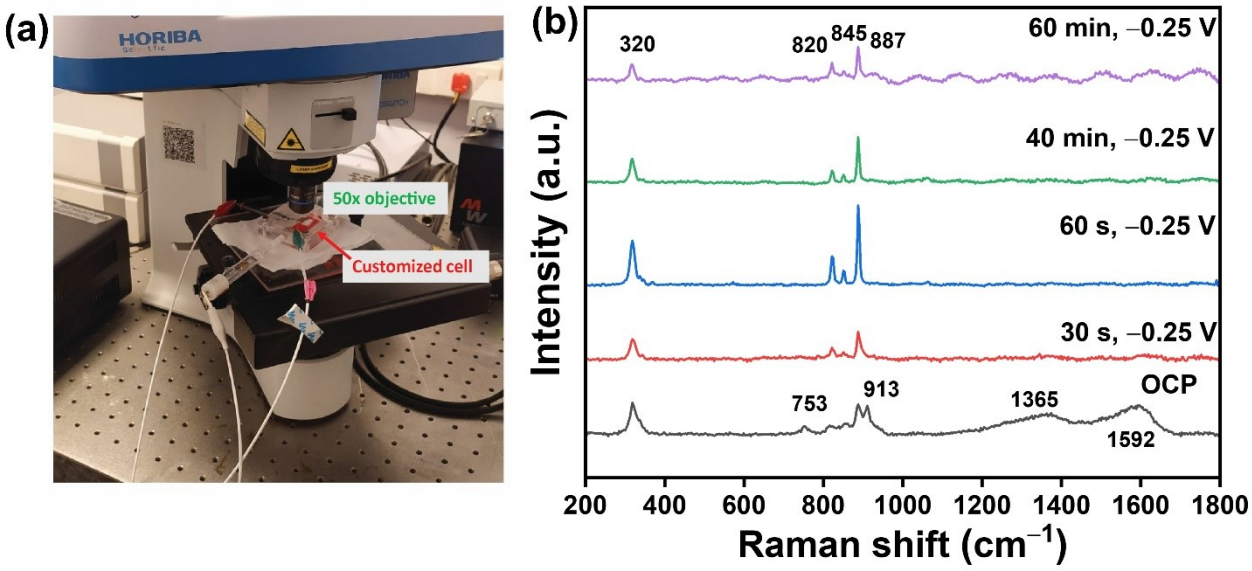

13. *In situ* Raman analysis

Figure S14. *(a) photographs of in situ Raman set-up (b) In situ Raman spectra of Mo_2C 730 at OCP and at the HER potential, −0.25 V for different time intervals in 1 M KOH.*

In situ Raman spectroscopy is performed to understand the structural transformation of the important catalyst, Mo_2C 730, during HER in 1 M KOH. In the absence of applied potential, i.e. at OCP, the characteristic peak observed at 753 cm^{-1} is ascribed to Mo-O vibrations of Mo-O-Mo functionalities of polymerised molybdate ions as mentioned in earlier studies[3,4]. Peaks ranging from 900-930 cm^{-1} are characteristic to MoO_4^{2-} in the wet state reported by *Helge Jeziorowski*[5]. The peak at 913 cm^{-1} is assigned to MoO_4 tetrahedra posing weak interactions with neighbouring groups through bridges with relatively longer Mo-O bonds. However, on applying a cathodic HER potential of −0.25 V vs. RHE, the two peaks at 753 cm^{-1} and 913 cm^{-1} have diminished. Notably, the three peaks at 320 cm^{-1}, 845 cm^{-1}, and 887 cm^{-1} which are the characteristic bond vibrations of MoO_4^{2-} species in alkaline media, remain constant.[6] The peaks at 845 cm^{-1}, 887 cm^{-1} and 320 cm^{-1} belong to asymmetric υ(Mo=O) stretching, symmetric υ(Mo=O) stretching, and bending vibrations of MoO_4 tetrahedral unit, respectively. In the scientific community, there are discrepancies about the origin of the peak at 820 cm^{-1} in Mo-based oxide systems. Cotton and wing[7] have attributed this peak to the stretching vibrational mode of bridging Mo-O, but with lack of certainty. In a separate investigation, Brown et al, have also assigned this peak to the stretching vibration of bridging Mo-O groups (interaction species). Nevertheless, Helge et al[5] suggested that band ranging from 700 to 850 cm^{-1} could indeed arise from the Mo-O-Mo bridging species but the only conclusive evidence

for the presence of bridging groups is the appearance of a peak near ~200 cm^{-1} (Mo-O-Mo deformation). In accordance with this claim, we have concluded that there is no Mo-O-Mo bridge species at a detectable level in the alkaline system, which is expected due to the poor stability of the polymolybdate species at higher values of pH[8], as already proven experimentally. In conclusion, since no Raman band near 200 cm^{-1} is observed in the present in case of Mo_2C 730 under potential, the band around 820 cm^{-1} band can be considered as a vibrational mode of distorted MoO_4^{2-}. So, no polymolybdate species are surmised to be existent during this electrochemical transformation.

14. ICP-OES data of electrolyte

Table S4. *ICP-OES of electrolytes after 20 h electrolysis in 1 M KOH (50 mL electrolyte)*

ICP-OES: Amount of Mo in the spent electrolyte		
Mo_2C 730	Mo/Mo_2C 930 2h	Mo/Mo_2C 930 4h
15.0 µg	182.0 µg	362.0 µg

15. ICP-OES analysis of Mo_2C 730

Table S5. *ICP-OES analysis of electrolytes of Mo_2C 730 for different HER durations*

ICP-OES: Amount of Mo in the spent electrolyte	
10 h	14.25 µg
20 h	15.0 µg
30 h	15.25 µg
40 h	25.5 µg

To evaluate the Mo leaching vs time during long-term operation, ICP-OES analysis of Mo_2C 730 was performed on the electrolyte after 10 h, 20 h, 30 h, and 40 h electrolysis (Table S4). The time-dependent analysis of Mo leaching, suggests an activation-stabilization process of the catalyst. The electrolyte analysis reveals a gradual accumulation of dissolved Mo species with time (14.25 µg, 15.0 µg, 15.25 µg, and 25.5 µg at 10 h, 20 h, 30 h and 40 h, respectively). During the initial 10 h, a relatively higher amount of Mo dissolution is observed, likely originating from surface-exposed or weakly coordinated Mo species that are immediately

accessible to the electrolyte, resulting in a temporary decrease in current density (−30.7 mA/cm^2 to −27.43 mA/cm^2). After 20 h and 30 h, Mo leaching increases only marginally, while the current density continues to rise (−34.87 mA/cm^2 at 20 h, −36.62 mA/cm^2 at 30 h) indicating that perhaps dissolution process is more limiting and coincides with electrochemical activation and surface reconstruction process. At extended operation (40 h), a further increase in dissolved Mo is observed (an additional ~10.25 µg), accompanied by a slight decrease in current density to −33.78 mA cm^{-2}. Nevertheless, despite this change, the catalyst is still able to sustain stable operation up to 47 h, indicating that the overall catalytic stability is maintained beyond the initial activation period.

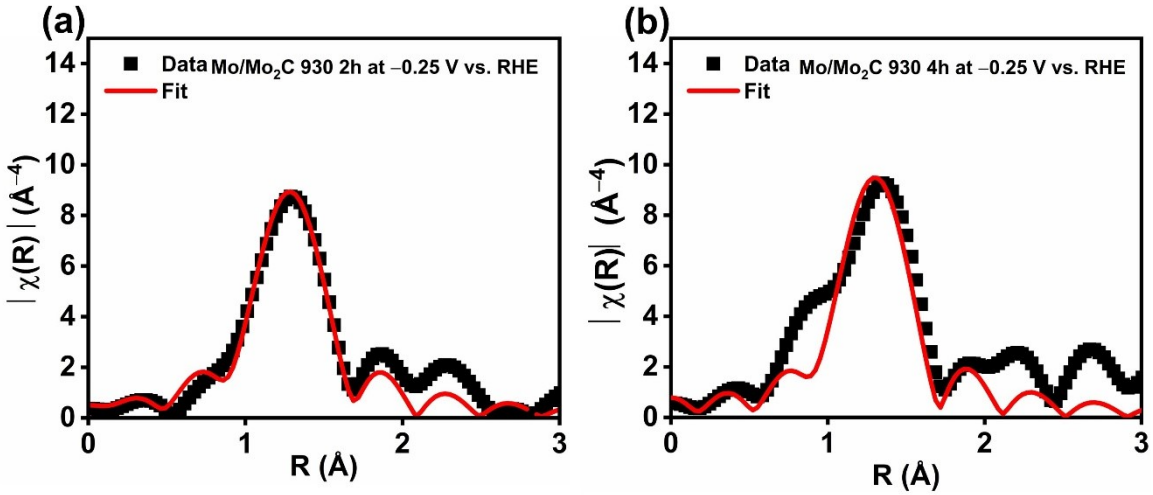

16. FT-EXAFS fitted graph

Figure S15. *(a) and (b) FT-EXAFS data and fitted graph of Mo/Mo$_2$C 930 2h and Mo/Mo$_2$C 930 4h at HER potential, −0.25 V in 1 M KOH.*

Table S6. *EXAFS fitting parameters of Mo/Mo_2C 930 2h and Mo/Mo_2C 930 4h at HER potential.*

	Path	CN	S_0^2	σ^2	E_0	delr (Å)	R (Bond distance) (Å)	R factor
Mo/Mo_2C 930 2h at HER potential	Mo-O	2.73 +/- 0.3054	1	0.00226 +/- 0.0012	−0.98	0.0177 +/-0.0091	1.7596	0.4 %
Mo/Mo_2C 930 4h at HER potential	Mo-O	2.87 +/- 0.8783	1	0.00261 +/- 0.0038	3.34	0.0239 +/- 0.0289	1.7658	2.6 %

[Fit range: $3 < k < 11$, $1 < R < 2$, CN = coordination number, S_0^2 = amplitude reduction factor, we fixed as 1 after fitting Mo foil, R = bond length of absorber (Mo), and scatter (O), σ^2 = mean squared disordered term, E_0 = energy shift, delr = change in interatomic distance relative to initial path length. The Mo-O scattering path taken from K_2MoO_4 system.]

17. Polarisation curves of bare GCE (glassy carbon electrode) in 0.5 M Na_2MoO_4 + 1 M KOH

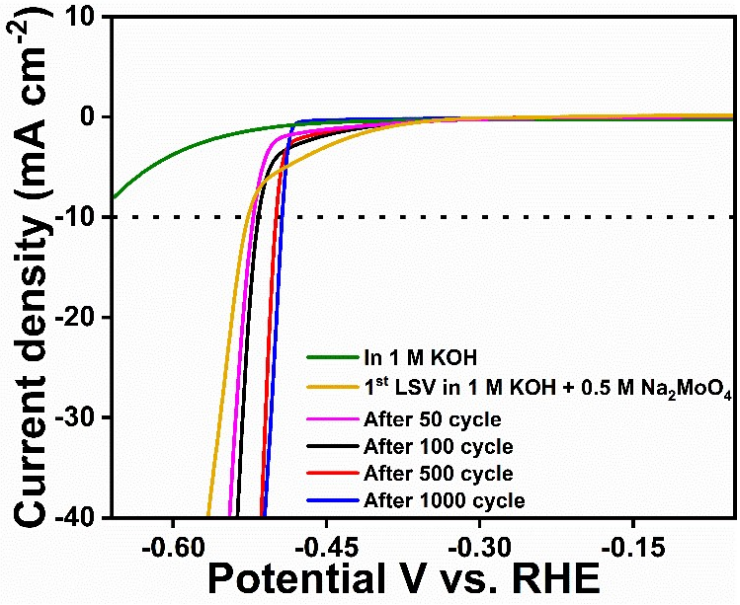

Figure S16. *LSV of bare GCE after performing potential cycling in in 0.5 M Na_2MoO_4 + 1 M KOH.*

18. Polarisation curves of Mo_2C 730 in 1 M KOH + Na_2MoO_4 (0.1 M, 0.2 M, 0.5 M)

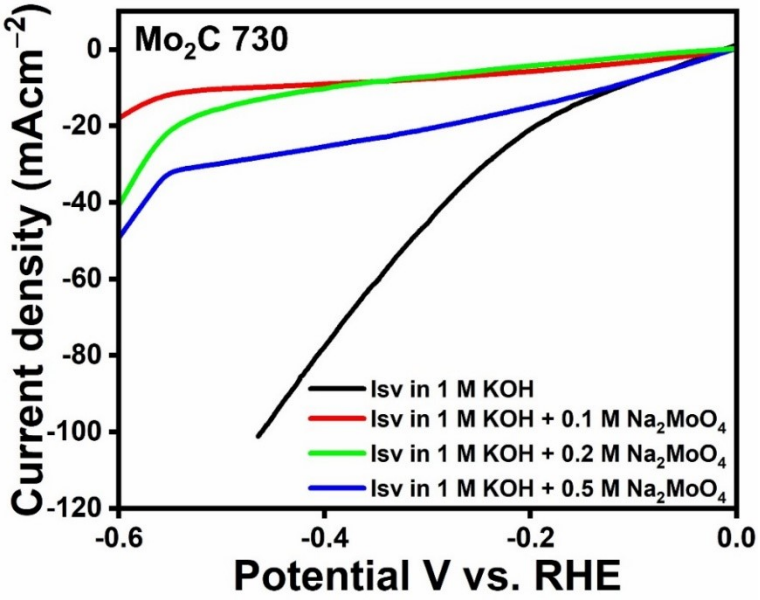

Figure S17. *LSV of Mo_2C 730 in various concentration of sodium molybdate solution (1 M KOH + (0.1, 0.2, 0.5 M Na_2MoO_4)).*

Role of MoO_4^{2-}:

To decouple the electrochemical role of molybdate $(MoO_4)^{2-}$ species from the intrinsic activity of the catalyst, polarization studies were carried out using re glassy carbon electrodes (GCE) in a molybdate-enriched alkaline electrolyte (1 M KOH + 0.5 M Na_2MoO_4). While an enhancement in HER was observed over GCE (493 mV @−10 $mAcm^{-2}$ after 1000 cycles) in the presence of molybdate relative to 1 M KOH (Fig. S17) still the activity remained

significantly lower than that of the various Mo_2C catalysts. 730 (117 mV @ 10 $mAcm^{-2}$), Mo/Mo_2C 930 2h (163 mV @ 10 $mAcm^{-2}$) and Mo/Mo_2C 930 4h (204 mV @ 10 $mAcm^{-2}$). This observation suggests that the HER enhancement in the studied catalysts cannot be attributed solely to the presence of $(MoO_4)^{2-}$ anions. So, another plausible explanation can be the catalyst effectively adsorbs $(MoO_4)^{2-}$species from the electrolyte under the applied potential, facilitating their reduction into MoO_x species, which could play a role in HER catalysis. To investigate this possibility, LSV measurements are performed for Mo_2C 730 in a 1 M KOH + (0.1 M, 0.2 M, 0.5 M) Na_2MoO_4.[9] The polarization curves clearly indicate that the addition of molybdate lowers the HER activity (requires <500 mV overpotential to initiate HER) (Fig. S18). Furthermore, a clear increase in pseudocapacitive current with increasing Na_2MoO_4 concentration is observed, indicating enhanced surface adsorption phenomena (Fig. S18). These findings suggest that the presence of $(MoO_4)^{2-}$ anions in the electrolyte may adsorb on to the catalyst surface, thereby inhibiting or blocking the formation of *in situ* generated MoO_x active species, which are believed to be responsible for HER activity. As a result, the HER onset potential shifts negatively, reflecting a suppression of catalytic activation. This supports the conclusion that the redeposition of $(MoO_4)^{2-}$or formation of polymeric Mo-species such as $(Mo_2O_7)^{2-}$ from the electrolyte does not contribute positively to the HER activity of Mo_2C-based catalysts.

19. XRD of Mo_2C 730 after stability

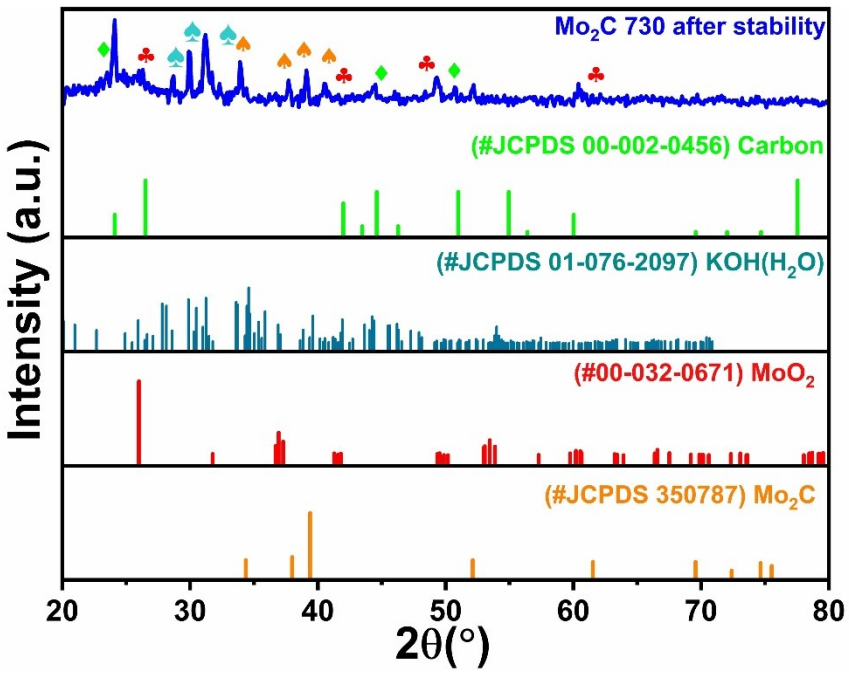

Figure S18. *Post-stability XRD of Mo_2C 730.*

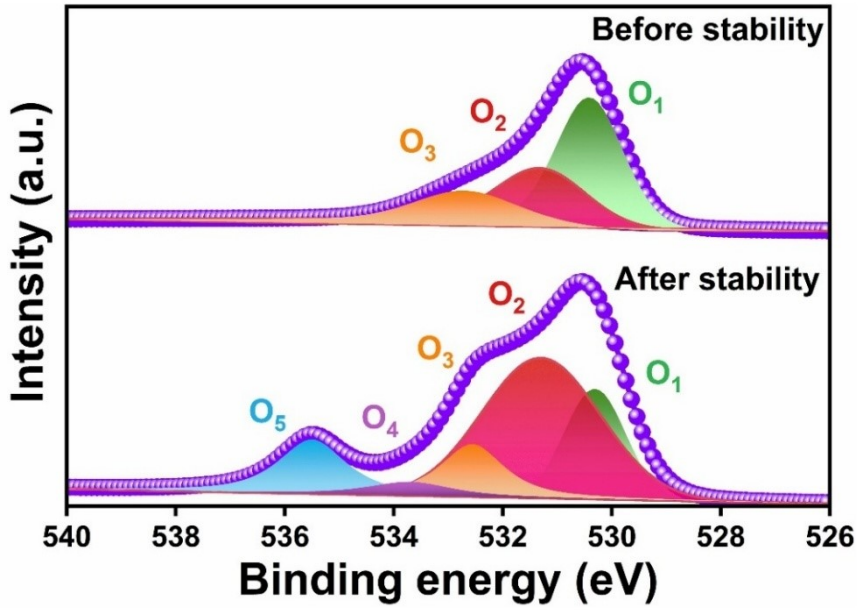

20. O 1S spectra of Mo_2C 730 after stability

Figure S19. *O 1S spectra of Mo_2C 730 before and after stability study.*

O3	532.5	
O4	533.7	
O5	532.5	

Table S7. *Surface oxygen species before and after HER stability for Mo_2C 730*

Table S8. *Relative concentration of Oxygen species from deconvoluted O 1S XPS spectra*

Catalysts	**O 1S**					**O_2/O_1**
Mo_2C 730	O_1 = 34.38%		O_2 = 33.12%	O_3 = 32.4%		**0.96**
Mo_2C 730 after stability	O_1 = 19.99%	O_2 = 21.18%	O_3 = 19.71%	O_4 = 19.35%	O_5 = 19.76%	**1.06**

21. Mo 3d spectra of Mo_2C 730 after stability

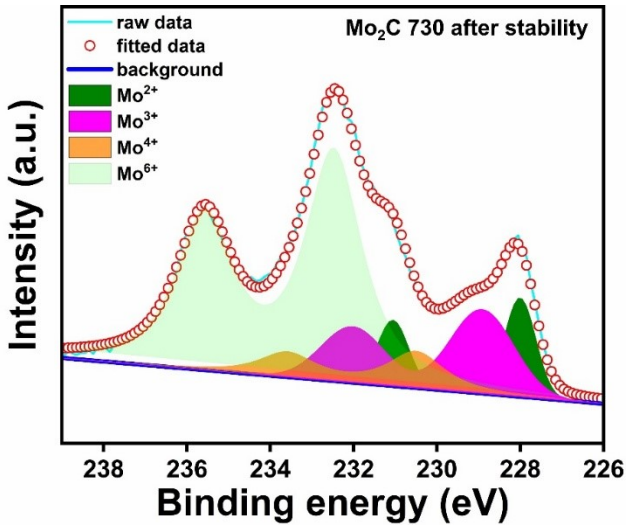

Figure S20. *Post-stability Mo 3d XPS spectra of Mo_2C 730.*

Table S9. *Elemental composition of Mo_2C 730 after stability and their relative percentage*

Catalyst	Species	B.E (eV) Mo $3d_{5/2}$	B.E (eV) Mo $3d_{3/2}$	Percentage (%)
Mo_2C 730	Mo^{2+}	228.0	231.05	21.05
	Mo^{3+}	228.91	232.01	23.35
	Mo^{4+}	230.5	233.6	20.57
	Mo^{6+}	232.48	235.58	35.02

22. EIS details after 20 h stability

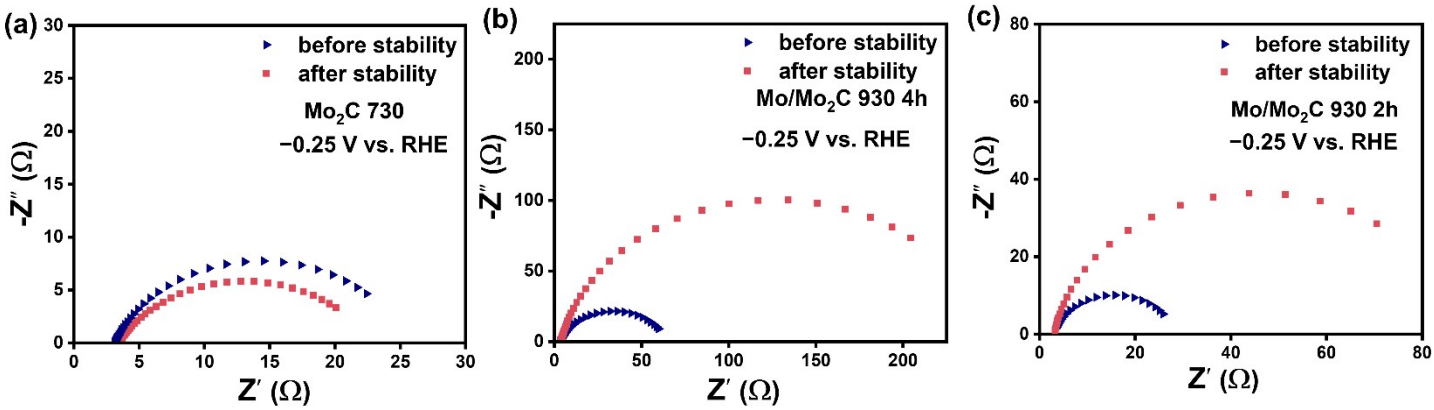

Figure S21.*Nyquist plot before and after 20 h stability Mo_2C 730, Mo/Mo_2C 930 2h, Mo/Mo_2C 930 4h on carbon paper.*

Table S10. *Impedance fitted data of Fig. S21, before and after stability study for various catalysts*

Catalysts		R_s (Ω)	R_{ct} (Ω)	CPE 1-T (F)	CPE 1-P (F) (10^{-3})	χ^2 (10^{-2})
Mo_2C 730	Before stability	3.10	22.52	3.6794×10^{-3}	0.76	0.2829
	After stability	3.41	19.35	3.6595×10^{-3}	0.70	0.051789
Mo/Mo_2C 930 2h	Before stability	3.17	27.51	3.2326×10^{-3}	0.79	4.731

	After stability	3.07	85.09	1.5561×10^{-3}	0.90	0.1767
Mo/Mo_2C 930 4h	Before stability	3.14	61.78	3.537×10^{-3}	0.78	0.50589
	After stability	3.67	246.1	1.7598×10^{-3}	0.87	0.29245

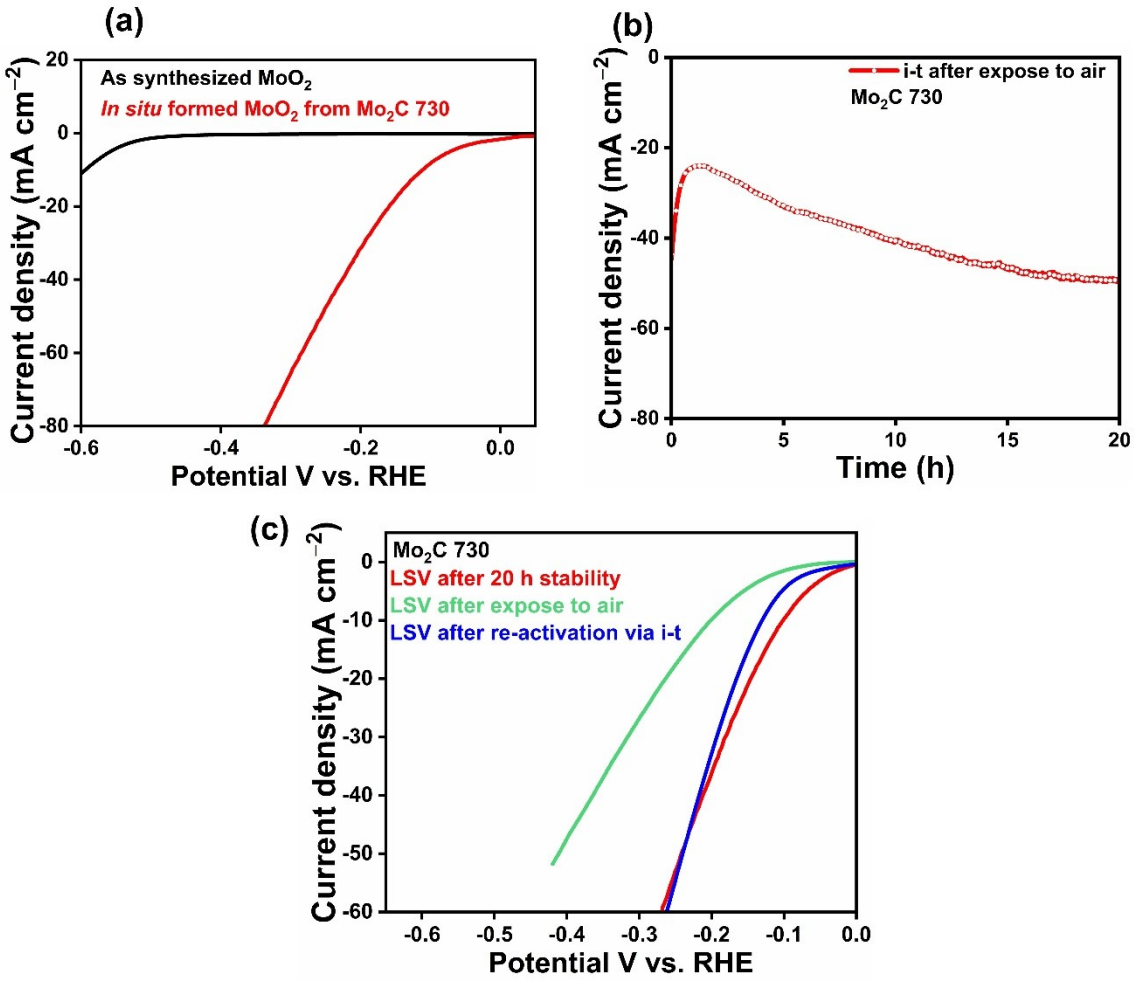

23. Electrochemical data for reactivation of Mo_2C 730

Figure S22. *(a) LSV comparison of standard MoO_2 (as prepared) and in-situ formed MoO_2 (defective) from Mo_2C 730. (b) 20h i-t at −0.25 V vs. RHE for activation of Mo_2C 730 after exposed to air (c) LSV of Mo_2C 730 after 20 h HER stability (red), exposed to air (green), after re-activation (blue).*

24. Details of theoretical calculations

Spin-polarized DFT calculations were carried out using the VASP package.[10–12] The exchange-correlation effects were treated using the generalised gradient approximation (GGA) with the Perdew-Burke-Ernzerhof (PBE) functional.[13] Long range van der Waals interactions were taken into consideration using Grimme's DFT-D3 correction.[14] The supercell structure with heterojunction interface was created by stacking MoO_2 (100) above Mo_2C (001). To suppress image interactions arising from periodic boundary conditions, a 15 Å thick vacuum was introduced along the z-direction. For the reciprocal space integration, Γ centred k-point mesh was used. A plane-wave cutoff energy of 500 eV was used in all calculations, along with an energy convergence tolerance of 10^{-5} eV and a convergence criterion of 0.01 eV/Å for each atomic force. The Fermi level Gaussian smearing factor was set at 0.05 eV. Rather than focussing on the interactions between substrate atoms, we primarily discuss the binding strength of HER intermediates on catalyst here. As a result, PBE+U correction is not considered.

The adsorption energy of H atom, E_{ads} on the substrates was calculated as

$$E_{ads} = E_{catalyst+H} - E_{catalyst} - \frac{1}{2}E(H_2)$$

The energy $E_{(catalyst+H)}$ denotes the energy of H adsorbed on catalyst ($Mo_2C@MoO_2$), $E_{(catalyst)}$ is the energy of the bare catalyst and $E(H_2)$ is the energy of the H_2 gas in a box.

The hydrogen adsorption free energy (ΔG_H) is a key indicator for efficiency of catalyst. For an effective catalyst, ΔG_H should be near to zero, suggesting an ideal balance between hydrogen adsorption and desorption. This is commonly achieved by computing the following equation.

$$\Delta G_H = E_{ads} + \Delta E_{ZPE} - T\Delta S_H \text{ ----- (1)},$$

where the zero-point energy change, determined from vibrational frequencies, is denoted by ΔE_{ZPE}. With the temperature (T) set to room temperature (298.15 K), the entropy (ΔS_H) characterizing the transition from the adsorbed state to the free-standing state is computed. From the database of the National Institute for Standards and Technology (NIST) the ΔS values for H_2 gas molecule is obtained.

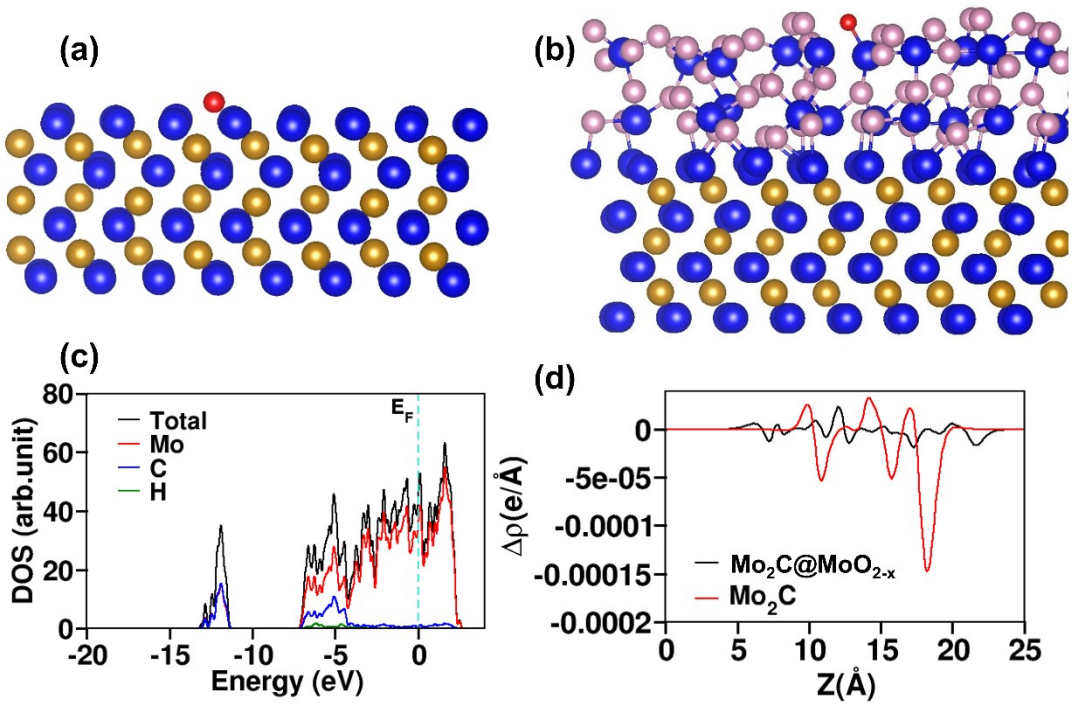

Figure S23.*H adsorbed on (a) (001) surface of Mo_2C and (b) on $Mo_2C@MoO_{2-x}$ heterojunction. (violet, red, golden yellow and blue colour represents O, H, C and Mo atom) (c) DOS plot of Mo_2C (001) (d) Plane-averaged electron density difference Δρ the black line corresponds to Δρ of $Mo_2C@MoO_{2-x}$ and the red line is for Mo_2C Δρ with respect to z.*

Table S11. *d-band centre of Mo and the Bader charge on H after adsorption on the surface*

Catalyst	*d*-band centre (eV)	Bader Charge on H	Bader Charge on Mo (Mo attached to H)
Mo_2C	−1.41	−1.02	1.46
$Mo_2C@MoO_{2-x}$	−1.57	−0.57	2.24

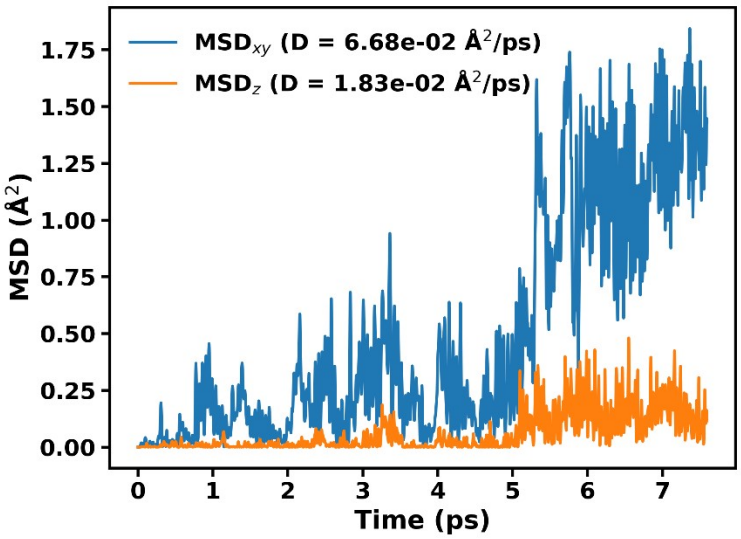

Figure S24. *MSD of hydrogen on $Mo_2C@MoO_{2-x}$ obtained from AIMD at 300 K. The dominant in-plane diffusion reflects low surface migration barriers, supporting the near-thermoneutral ΔG_H and accelerated hydrogen evolution kinetics.*

AIMD simulations can capture the initial stages of surface reconstruction and assess the thermal stability of intermediates under finite-temperature conditions. While the limited AIMD timescale does not permit direct observation of carbide-to-oxide transformation or oxygen incorporation, the simulations demonstrate that the reconstructed $Mo_2C@MoO_{2-x}$ surface is dynamically stable at 300 K and supports facile surface hydrogen diffusion. These results are consistent with the experimentally observed self-limited surface reconstruction inferred from *in situ* XAS and Raman spectroscopy, and with DFT-predicted hydrogen adsorption.

The mean squared displacements (MSDs) of all atoms were computed with this structure based on the NVT. Using MSD, it is feasible to estimate the average movement of a set of atoms as a function of time, and it is calculated as

$$MSD = \frac{1}{N}\sum_{i=0}^{N}(r_i(t) - r_i(0))^2$$

where $r_i(0)$ and $r_i(t)$ are the position of atoms at initial (i.e at t=0) and final (i.e at t=t) positions of a given atom, respectively, and N is the number of atoms.

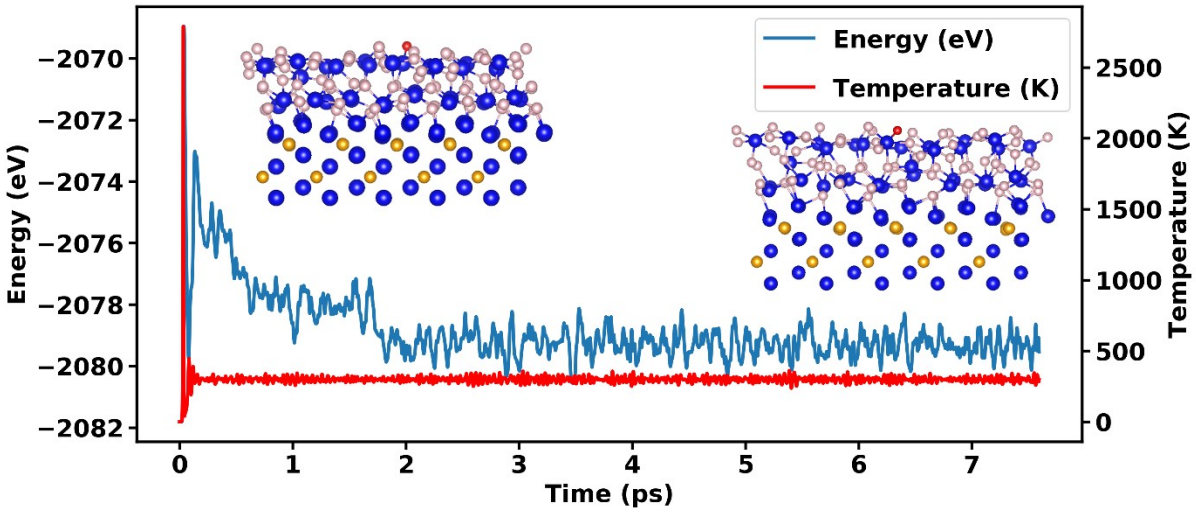

Figure S25. *AIMD-derived total energy and temperature fluctuations as a function of simulation time at 300 K, indicating dynamic stability of the hydrogen-adsorbed $Mo_2C@MoO_{2-x}$ heterostructure.*

References:

1 K. K. Singh, V. Ramakrishnan, R. Prabhu B. and N. S. John, *CrystEngComm*, 2017, **19**, 6568–6572.

2 J. Fan, X. Wu, A. Piñeiro-García, N. Boulanger, Y. Panecatl-Bernal, A. Ashok, S. Koroidov and E. Gracia-Espino, *ACS Appl. Nano Mater.*, 2021, **4**, 12270–12277.

3 H. Tian, C. A. Roberts and I. E. Wachs, *J. Phys. Chem. C*, 2010, **114**, 14110–14120.

4 V. V Popov, A. P. Menushenkov, A. A. Yastrebtsev, A. Yu. Molokova, A. A. Pisarev, E. V Khramov, Y. V Zubavichus, I. V Shchetinin, K. V Ponkratov, N. A. Tsarenko and N. V Ognevskaya, *J. Solid State Chem.*, 2021, **301**, 122356.

5 H. Jeziorowski and H. Knoezinger, *J. Phys. Chem.*, 1979, **83**, 1166–1173.

6 F. D. Hardcastle and I. E. Wachs, *J. Raman Spectro.*, 1990, **21**, 683–691.

7 F. A. Cotton and R. M. Wing, *Inorg. Chem.*, 1965, **4**, 867–873.

8 H. Hu, I. E. Wachs and S. R. Bare, *J. Phys. Chem.*, 1995, **99**, 10897–10910.

9 W. Du, Y. Shi, W. Zhou, Y. Yu and B. Zhang, *Angew. Chem. Int. Ed.*, 2021, **60**, 7051–7055.

10 G. Kresse and J. Hafner, *Phys. Rev. B*, 1993, **47**, 558–561.

11 G. Kresse and J. Furthmüller, *Phys. Rev. B*, 1996, **54**, 11169–11186.

12 G. Kresse and J. Furthmüller, *Comput. Mater. Sci.*, 1996, **6**, 15–50.

13 J. P. Perdew, K. Burke and M. Ernzerhof, *Phys. Rev. Lett.*, 1996, **77**, 3865–3868.

14 S. Grimme, S. Ehrlich and L. Goerigk, *J. Comput. Chem.*, 2011, **32**, 1456–1465.